ARTICLES
https://doi.org/10.1038/s41560-020-00757-7

nature energy

Check for updates

Thermally modulated lithium iron phosphate batteries for mass-market electric vehicles

Xiao-Guang Yang[1], Teng Liu[1] and Chao-Yang Wang[1,2]✉

The pursuit of energy density has driven electric vehicle (EV) batteries from using lithium iron phosphate (LFP) cathodes in early days to ternary layered oxides increasingly rich in nickel; however, it is impossible to forgo the LFP battery due to its unsurpassed safety, as well as its low cost and cobalt-free nature. Here we demonstrate a thermally modulated LFP battery to offer an adequate cruise range per charge that is extendable by 10 min recharge in all climates, essentially guaranteeing EVs that are free of range anxiety. Such a thermally modulated LFP battery designed to operate at a working temperature around 60 °C in any ambient condition promises to be a well-rounded powertrain for mass-market EVs. Furthermore, we reveal that the limited working time at the high temperature presents an opportunity to use graphite of low surface areas, thereby prospectively prolonging the EV lifespan to greater than two million miles.

The transportation sector accounts for 29% of US greenhouse gas emissions, 59% of which come from light-duty vehicles making personal trips[1]. Powertrain electrification is a promising route for decarbonized transportation[2]. In light of the Paris Agreement, many countries have announced plans to phase out internal combustion engine (ICE) vehicles and incentivize electric vehicles (EVs). Driven by government policy and by rapid advances in battery technology, global passenger EV sales soared from a few thousand in 2010 to 2.1 million in 2019, and are projected to reach 8.5 million in 2025 and 54 million (58% of new car sales) in 2040[3]. On this cusp of massive EV adoption, global automakers are planning an unprecedented level of investment (at least US$300 billion in the next five years[4]) to develop batteries and EVs.

The pursuit of higher battery energy density to eliminate range anxiety has been the primary focus for EV battery development in the past decade[5–7]. Electric vehicle batteries have shifted from using lithium iron phosphate (LFP) cathodes to ternary layered oxides (nickel–manganese–cobalt (NMC) and nickel–cobalt–aluminium (NCA)) due to the higher energy density of the latter[8–10]. The global market share of ternary batteries reached a record high of 90% in 2019[11], and it was widely believed that future EV batteries would converge on ternary cathodes increasingly rich in nickel, as a higher nickel content renders a larger specific capacity and less demand for expensive cobalt[12,13].

However, a critical issue of nickel rich cathodes is poor safety due to the deterioration of thermal stability with increasing nickel content[14–17]. For instance, the onset temperature for self-sustained exothermic reactions drops from 306 °C for NMC111 (33% nickel) to 260 °C for NMC622 (60% nickel) and 232 °C for NMC811 (80% nickel)[18]. Heat release, on the other hand, increases from 512.5 J g^{-1} for NMC111 to 721.4 J g^{-1} for NMC622 and 904.8 J g^{-1} for NMC811. Furthermore, deformation of an NMC lattice at a high voltage releases oxygen, posing a considerable risk of thermal runaway. In comparison, LFP has a wide but flat exothermic reaction peak at 250–360 °C with a much smaller heat release of 147 J g^{-1} (ref. [19]), and the strong P–O covalent bond prohibits oxygen release[20], thus exhibiting intrinsic safety. Tests from Sandia National Laboratories[21] showed that a ten-cell LFP module had only limited temperature rise (peak temperature <79 °C) on nail penetration. A similar test on a seven-cell NMC module caused fires in all cells with a peak temperature of 549 °C. Wang and colleagues[22] compared the fire hazards of 80 Ah LFP and 50 Ah NMC cells by triggering thermal runaway with a resistive heater and found that the NMC cell had 2.9 times the heat release rate and three times the toxic CO release than the LFP cell. A recent report[23] from China's National Big Data Alliance of New Energy Vehicles showed that 86% EV safety incidents reported in China from May to July 2019 were on EVs powered by ternary batteries and only 7% were on LFP batteries.

Lithium iron phosphate cells have several distinctive advantages over NMC/NCA counterparts for mass-market EVs. First, they are intrinsically safer, which is the top priority of an EV. Second, the use of LFP cells has brought the battery pack cost down[24,25] to below US$100 per kWh, a critical threshold for EVs to reach cost parity with ICE cars. The cost of NMC/NCA packs, however, is around US$156 per kWh as of 2019[3] and it will be challenging to reduce this cost to US$100 per kWh any time soon. Third, LFP materials are highly durable, rendering long battery life[26]. Fourth, LFP has no cobalt, a strategic metal whose sustainable supply is highly questionable[13]. As such, LFP cells are promising for widespread adoption in mass-market passenger EVs. The main barrier, however, is the low energy density due to the limited specific capacity and discharge voltage, which causes severe range anxiety. State-of-the-art LFP cells have a specific energy of ~180 Wh kg^{-1}, whereas NMC and NCA cells have reached >250 Wh kg^{-1}. Nonetheless, this gap in energy density has been much narrowed at the pack level by recent advances in cell-to-pack (CTP) technology. One example is the blade battery recently unveiled by BYD[27], where single cells are as long (600–2,500 mm) as the pack and hence the cell-to-pack integration efficiency is 40% higher, resulting in similar specific energy and even better energy density at the pack level of a LFP battery compared to a ternary battery.

Although the much-improved CTP efficiency helps revisit LFP batteries, mass-market passenger EVs truly free of range anxiety still require key technological breakthroughs. Here we present a thermally modulated LFP (TM-LFP) blade battery designed to operate at an elevated temperature of around 60 °C. Working

[1]Department of Mechanical Engineering and Electrochemical Engine Center, The Pennsylvania State University, University Park, PA, USA. [2]EC Power, State College, PA, USA. ✉e-mail: cxw31@psu.edu

at 60 °C not only tackles the low-temperature issues of the LFP chemistry but also considerably boosts kinetic and transport properties, giving rise to 10 min fast charging and remarkable power in all climates. We note that speedy, convenient replenishment of on-board battery energy through 10 min recharge is a cheaper and safer alternative than highly energy-dense batteries or loading up sheer size batteries to eliminate range anxiety for mass-market passenger EVs. Besides, we show that the elevated operating temperature greatly simplifies battery thermal management due to a 14-fold reduction in the need for battery cooling, further enhancing the energy density of the LFP battery system beyond—and reducing cost below—that of the CTP technology. Furthermore, the high operating temperature with a limited exposure time makes it viable to utilize graphite with low Brunauer–Emmett–Teller (BET) areas, which can prolong battery life to greater than two million driving miles. On the whole, the TM-LFP blade battery can fulfil all of the main criteria required for EVs—that is, that they are low cost, ultra-safe, recharge quickly (to be free of range anxiety), are weather independent and have a long lifetime—and thus exhibit enormous potential for large-scale adoption in the upcoming mass-market passenger EVs.

Cell-to-pack integration

Aside from cell-level energy density, another crucial factor affecting the cruise range of an EV is the integration efficiency from cells to a pack. A conventional battery pack consists of multiple modules, each having numerous single cells (Fig. 1a). The mass and volume of the cells are only part of that of the pack. We performed a survey of the specific energy (gravimetric) and energy density (volumetric) of commercial EV batteries at cell and pack levels, as presented in Fig. 1c,d (see Supplementary Table 1 for details). Notably, most EVs have a gravimetric cell-to-pack ratio (GCTP; that is, the ratio of specific energy at the pack level to that at cell level) of around 0.55–0.65, meaning 35–45% of pack weight is taken by inactive elements (battery management system, thermal management system, metal cases, cabling, beams and so on). The volume efficiency is more disappointing: the volumetric cell-to-pack ratio (VCTP) of most EVs are below 0.4. To improve mass and space utilization, several battery suppliers such as CATL and BYD have adopted so-called CTP technology, which removes modules and directly assembles cells into a pack. An example is the blade battery recently unveiled by BYD[27]. As schematically illustrated in Fig. 1b, a blade battery pack builds on an array of wide (600–2,500 mm) and short cells having a similar width as the pack. All module-related parts are removed, and the cells themselves can provide structural support so that heavy beams used in a conventional battery pack for holding modules are saved as well. As such, the blade battery pack in the newly unveiled BYD Han EV achieves an outstanding GCTP of 0.85 and VCTP of 0.62, giving rise to similar specific density and even better energy density at the pack level compared with EVs with ternary batteries (Fig. 1c,d).

LFP blade battery

Here we evaluate the performance of LFP blade batteries under various performance criteria required for EVs. Specifically, we compare graphite-LFP cells in blade battery format (following the dimensions from BYD[27]) with conventional graphite-NMC622 cells in prismatic format (VDA-BEV2 standard, the same dimensions as the cells in BMW i3). Detailed cell design information is summarized in Supplementary Table 2. The two types of cells are compared in terms of energy and power densities, cruise range under both city and highway driving scenarios, and fast-charging ability—all under various ambient temperatures. Electrochemical–thermal (ECT) models calibrated over a wide range of testing conditions (Supplementary Figs. 1–4) are used to perform the comparison, as detailed in the Methods. It should be noted that efficient operation of blade batteries necessitates multitab or 'tab everywhere' design to minimize voltage loss along the foil length and ensure uniform current distribution. Many such designs have been elaboratively presented in the patent literature[28–30], resulting in very comparable internal resistance of blade batteries to traditional short cells. This is assumed in the present work without sketching the tab design in Fig. 1b for simplicity. A detailed electron flow analysis along the cell length can be found in Supplementary Note 1.

The most common approach to enhance the energy density of a lithium ion cell is to increase the areal loading of the electrodes[31]. Figure 2 presents the specific energy and energy density of the LFP and NMC622 cells under the fixed cell dimensions (Supplementary Table 2). As expected, the LFP cells have lower specific energy and energy density than the NMC622 cells (Fig. 2a,c), but this deficiency can be compensated by the high CTP ratios of the blade battery pack (Fig. 2b,d). At the loading of 4 mAh cm^2, for instance, the pack-level specific energy of the LFP blade battery reaches 156–175 Wh kg^{-1} at a GCTP of ~0.8–0.9, compared with 145–171 Wh kg^{-1} for the conventional NMC622 pack at a GCTP of ~0.55–0.65. The improvement in volumetric energy density is more exciting. The LFP blade battery pack at 4 mAh cm^{-2} loading achieves an energy density of 286–333 Wh l^{-1} at a VCTP of ~0.6–0.7, which is much higher than that of the conventional NMC622 pack (186–249 Wh l^{-1} at a VCTP of ~0.3–0.4). It can be concluded that a blade-type LFP battery pack can deliver specific energy comparable to and energy density even higher than a state-of-the-art ternary battery pack (also compare with Supplementary Table 1).

Peak battery power is vital for EVs, which represents the ability for acceleration or regenerative braking. In the recently published battery requirements for 2030 mass-market EVs[32], the European Council for Automotive R&D (EUCAR) set a target of 1,440 W kg^{-1} for peak (10 s) specific power and 3,000 W l^{-1} for peak power density at the pack level in the state-of-charge (SOC) range of 10–100%. Here we compare the power of the LFP blade cell and NMC622 VDA cell with the areal capacity of 3 mAh cm^{-2} (see Supplementary Table 2 for details; the discussion in the remainder of this work is based on these two cells unless otherwise noted). The power density is assessed by a 10 s discharge pulse at a constant voltage that equals the lower cutoff voltage (2.4 V for the LFP cell and 2.7 V for the NMC622 cell). Supplementary Figs. 5 and 6 present the specific power and power density of the two batteries at the cell and pack levels under various temperatures and SOCs. Notably, a critical challenge to battery power is low temperature, as we can see that both cells suffer an exponential drop in power with decreasing temperature. As EVs need to operate in all weather conditions, boosting battery power at low temperatures is vital for ensuring a pleasant driving experience. On the other hand, we note that an increase in temperature can enhance battery power substantially. If operating at 60 °C, for instance, the specific power and power density of the LFP blade battery can readily meet the EUCAR 2030 target even at 10% SOC (Supplementary Figs. 5f and 6f).

The cruise range is the most crucial metric for an EV, which we evaluate here for an EV powered by a 40 kWh battery pack (composed of either 62 of the 202 Ah LFP blade cells or 69 of the 158 Ah NMC622 VDA cells in Supplementary Table 2). One example of such an EV is the Nissan Leaf. We study two scenarios, city driving and highway driving, respectively, by following the Urban Dynamometer Driving Schedule (UDDS) and US06 high acceleration aggressive driving schedule defined by the US Environmental Protection Agency (EPA)[33]. The EPA-defined velocity profiles are converted to battery power profiles (Supplementary Fig. 7) through a vehicle dynamics model that is based on the specifications of Nissan Leaf, as detailed in the Methods.

Figure 3a,b displays the voltage profiles of the LFP and NMC622 cells under the above-mentioned driving schedules at different temperatures, whereas Fig. 3c,d summarizes the

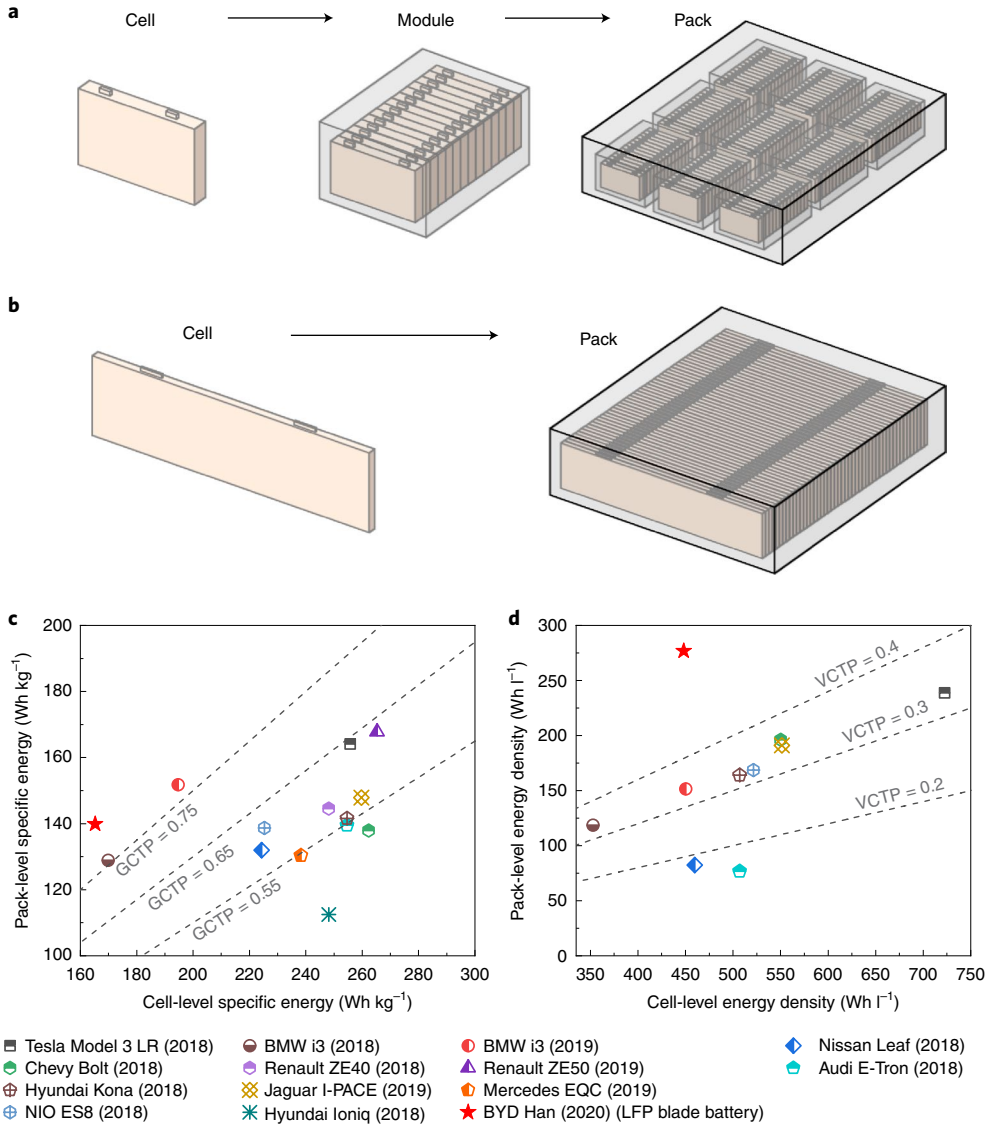

Fig. 1 | Cell-to-pack technology. a,**b**, A schematic illustration of a conventional battery pack (**a**) and a blade battery pack (**b**). The conventional battery pack uses cells to build a module and then assembles modules into a pack. A blade battery pack builds on wide and short cells and assembles them directly into a pack, thereby having much higher mass and volume integration efficiencies than the conventional pack. **c,d,** A summary of the pack- and cell-level gravimetric specific energy (**c**) and volumetric energy density (**d**) of the battery packs in state-of-the-art EVs. All parameters of the battery cells and packs needed to calculate these data points, along with the corresponding references, are summarized in Supplementary Table 1.

corresponding driving range. Under UDDS protocol, the driving range with the two batteries is similar at warm temperatures (decreasing moderately from 290 km at 60 °C to 270 km at 10 °C). At freezing temperatures, however, the cruise range descends rapidly, especially for the EV with the LFP blade battery whose range falls to 158 km at −10 °C and 39 km at −20 °C, as compared with 228 km at −10 °C and 157 km at −20 °C for the EV with the NMC622 battery. The sharp reduction in the cruise range of the LFP battery-powered EV can be attributed to the high mass-transfer resistance in the thick LFP cathode. At the same areal capacity of 3 mAh cm^{-2}, the thickness of the LFP cathode is 1.6 times that of the NMC622 cathode (Supplementary Table 2). As electrolyte conductivity and diffusivity drop substantially at low temperatures, the thick LFP cathode suffers much higher ionic resistance (Supplementary Fig. 8a) and greater electrolyte transport resistance (Supplementary Fig. 8b). Only half of the LFP cathode in the vicinity of the separator can therefore be fully lithiated at the end of the UDDS cycling at −10 °C (as shown in Supplementary Fig. 8c) whereas the lithiation degree of the NMC622 cathode is quite uniform.

The temperature effects on cruise range are more dramatic in highway driving scenarios. Under the US06 protocol, as shown in Fig. 3b,d, the driving range with the LFP battery falls to only 58% of the driving range with the NMC622 battery at 0 °C, and this ratio drops further to 30% at −10 °C. Such greater temperature effects are attributed to the higher power demand for highway driving, which induces a larger electrolyte concentration gradient in the thick LFP cathode (Supplementary Fig. 8e). Accordingly, only one-fifth of the LFP cathode can be fully lithiated at the end of the US06 cycling at −10 °C (Supplementary Fig. 8f).

Besides, we should note that regenerative braking, which accounts for ~28% of the cruise range under UDDS protocol and ~20% under US06 protocol, is typically prohibited at low temperatures as it can induce lithium plating (Supplementary Fig. 9); thus, only the solid bars in Fig. 3c,d should be considered as the driving range at <0 °C, making the cruise range even lower at freezing temperatures.

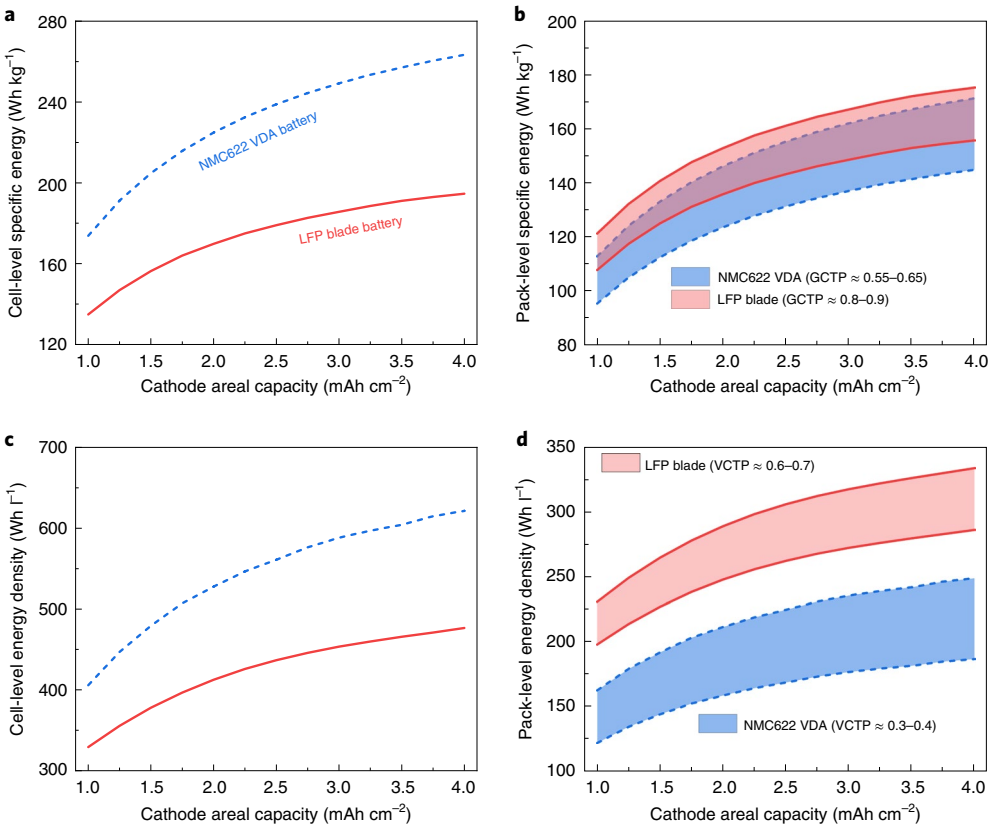

Fig. 2 | Specific energy and energy density at cell and pack levels. a–d, The evolutions of the gravimetric-specific energy (**a**,**b**) and volumetric energy density (**c**,**d**) of the LFP blade battery and NMC622 prismatic battery (VDA-BEV2 standard) at cell (**a**,**c**) and pack (**b**,**d**) level as a function of cathode areal capacity. Both cells are under the fixed cell dimensions given in Supplementary Table 2. In all cases the anode and cathode porosities are fixed at 0.27, and the negative-to-positive capacity ratio is fixed at 1.1.

Fast charging is widely recognized as the key to eliminating range anxiety. The US Department of Energy has identified 10 min extreme fast charging as a crucial enabler of mainstream EV adoption. The fundamental limitation of fast charging is lithium plating, which can drastically reduce battery life and even induce safety hazards. Figure 4 displays the cell voltage and anode potential (at the anode–separator interface) of the LFP and NMC622 cells during charging at different C-rates and temperatures. A standard constant-current–constant-voltage (CCCV) protocol is adopted with an upper cutoff voltage of 3.65 V for the LFP cell and 4.2 V for the NMC622 cell. As the two cells have the same anode design, their anode potential profiles overlap in the initial constant current charging step. Due to a lower upper voltage, the LFP cell enters the constant voltage step earlier than the NMC622 cell, which leads to a longer charging time (at the same C-rate) but prevents a further drop of the anode potential. As such, the LFP cell is less susceptible to lithium plating and therefore can be charged with a higher rate than the NMC622 cell. For instance, the LFP cell can withstand 3C charging at 25 °C, whereas the NMC622 cell can only take 1.5C.

We note from Fig. 4 that temperature has a substantial impact on the plating-free maximum charge rate (PF-MCR) of both cells (see also Supplementary Fig. 10). The PF-MCR refers to the maximum charge C-rate required for the anode potential to stay above 0 V. We can see that the PF-MCR at 0 °C drops to 0.7C for the LFP cell and 0.4C for the NMC622 cell, prolonging the charging time (0–80% SOC) to 80 min for the LFP cell and 112 min for the NMC622 cell (Fig. 4d). On the other end, elevating cell temperature can boost the fast-charging ability substantially. At 60 °C, the PF-MCR rises to 4C for the NMC622 cell and to >6C for the LFP cell (Fig. 4f). The LFP cell at 60 °C has no lithium plating even when charging with an aggressive protocol of CV at 3.65 V throughout the process. Under such a protocol, it takes only 9.4 min to charge from 0 to 80% SOC.

It can be concluded that LFP blade batteries—with their high CTP ratios—can deliver comparable specific energy and better energy density at the pack level to NMC batteries; LFP cells are also less susceptible to lithium plating and hence can be charged faster than NMC cells. The most critical challenge to LFP batteries for adoption in passenger EVs is the sharp reduction in cruise range at freezing temperatures due to the high mass-transfer resistance in the thick LFP cathodes. Besides, similar to NMC batteries, LFP cells face the issues of much-reduced power and rechargeability at low temperatures.

TM-LFP blade battery

We believe that a LFP battery of decent energy density at the pack level, as elaborated above, coupled with a 10 min fast rechargeability, is an economical solution to mass-market passenger EVs. To this end, we propose a TM-LFP blade battery designed to operate at an elevated temperature of 60 °C in any ambient condition. In practice, this can be implemented by rapid heating before battery operation (EV driving), which is feasible as long as the heating speed is fast. For instance, we reported a self-heating lithium ion battery structure with an embedded nickel foil as an internal heater[34], which achieves a heating speed greater than 1 °C per second, meaning that, even in the extreme cold of −30 °C, it takes only 90 s for the battery to warm up to 60 °C before operation (driving). The added weight and cost due to the introduction of nickel foils are negligibly small, estimated to be 1.3% drop in specific energy and 0.47% increase in cost[35,36]. Furthermore, this cell structure has been demonstrated viable for mass production and has already been utilized in real-world EVs[37].

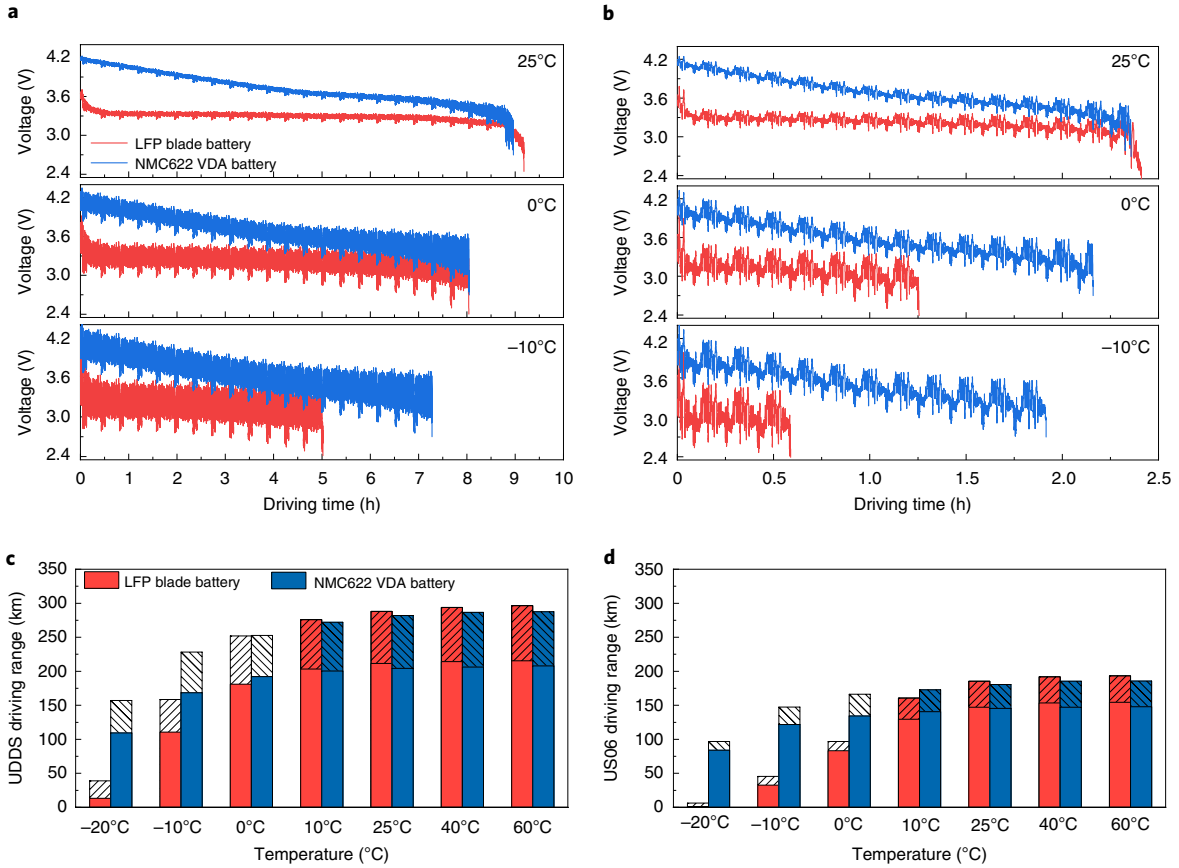

Fig. 3 | Cruise range under city and highway driving in different temperatures. a–d, A comparison of the driving behaviour of an EV (similar to a Nissan Leaf) powered by a 40 kWh battery pack composed of either the LFP blade cells or the NMC622 prismatic cells (VDA-BEV2 standard). The cell voltage (**a**,**b**) and total driving range (**c**,**d**) at different temperatures are shown. Results in **a** and **c** are under the UDDS protocol, which represents a city-driving scenario, whereas results in **b** and **d** are under the US06 protocol, representative of highway driving. The solid bars in **c** and **d** represent the driving range without regenerative braking (replacing the positive values of power in Supplementary Fig. 7 with zero), and the sum of solid and dashed bars represents the driving range with incorporation of regenerative braking. Note that regenerative braking at <0 °C is typically prohibited due to the issue of lithium plating (Supplementary Fig. 9).

Operating at an elevated temperature is quite beneficial as the performance of a lithium ion cell is fundamentally affected by the rates of the following physicochemical processes: electrochemical reactions at the surfaces of anode and cathode materials, lithium ion conduction and diffusion in the electrolyte, and solid-state lithium diffusion in anode and cathode particles. Key parameters that govern these processes all depend strongly on temperature, following the Arrhenius law (Supplementary Fig. 11). For instance, LFP materials are known for having the issue of poor solid-state diffusivity and have to be made into nanoparticles for use in lithium ion cells. Elevating temperature from 20 °C to 60 °C can boost the solid-state diffusivity of LFP by 60-fold (Supplementary Fig. 11) and thereby can substantially mitigate the lithium diffusion resistance in LFP particles. All of the aforementioned physicochemical processes accelerate at the elevated temperature of 60 °C, which can bring numerous benefits to an EV, as detailed below.

First, operating a cell consistently at 60 °C prevents the sharp drop in cruise range at low ambient temperatures, which, as idendified above, is the most critical barrier to LFP blade batteries. Supplementary Fig. 12 shows the voltage profiles of a 40 kWh TM-LFP battery pack under the UDDS driving cycle at freezing temperatures. The TM-LFP battery is preheated to 60 °C before driving, which consumes about 1.35% battery energy per 10 °C temperature rise according to the previous test results of cells with similar specific energy[38]. This energy consumption is used to reset the initial SOC of the TM-LFP battery for the UDDS cycle (for example, it starts at 89.2% SOC in the case of −20 °C ambient). Despite the energy consumption for heating, we can see that the TM-LFP battery has much smaller voltage oscillations (that is, lower cell resistance) and sustains much longer driving than regular LFP and NMC cells that start the discharge at 100% SOC. Figure 5a summarizes the driving range (calculated by integrating the UDDS velocity profile in Supplementary Fig. 7a over the driving time) at different temperatures. We can note that the TM-LFP battery enables a decent cruise range at all ambient conditions. At warm temperatures, the cruise range is about 290 km (note that this range can be extended to 400 km if the battery is scaled up to 50–55 kWh). At cold temperatures (for instance, −20 °C), despite the 10.8% battery energy consumed for preheating, the TM-LFP battery still delivers a range of 260 km, which is far superior to the range with the regular LFP blade battery (13 km) and with the conventional NMC622 battery (110 km) at the −20 °C ambient. The TM-LFP battery is thus able to deliver adequate cruise range per charge in all climatic conditions.

Second, the TM-LFP battery exhibits extraordinary power at all ambient temperatures. As shown in Supplementary Figs. 5 and 6, battery power drops exponentially with decreasing temperature, posing a critical challenge to vehicle acceleration and regenerative braking in cold weather. By operating consistently at 60 °C, battery power, on the one hand, becomes independent of ambient temperature (Fig. 5b), whereas on the other it is further boosted by 2.4-fold (compared with

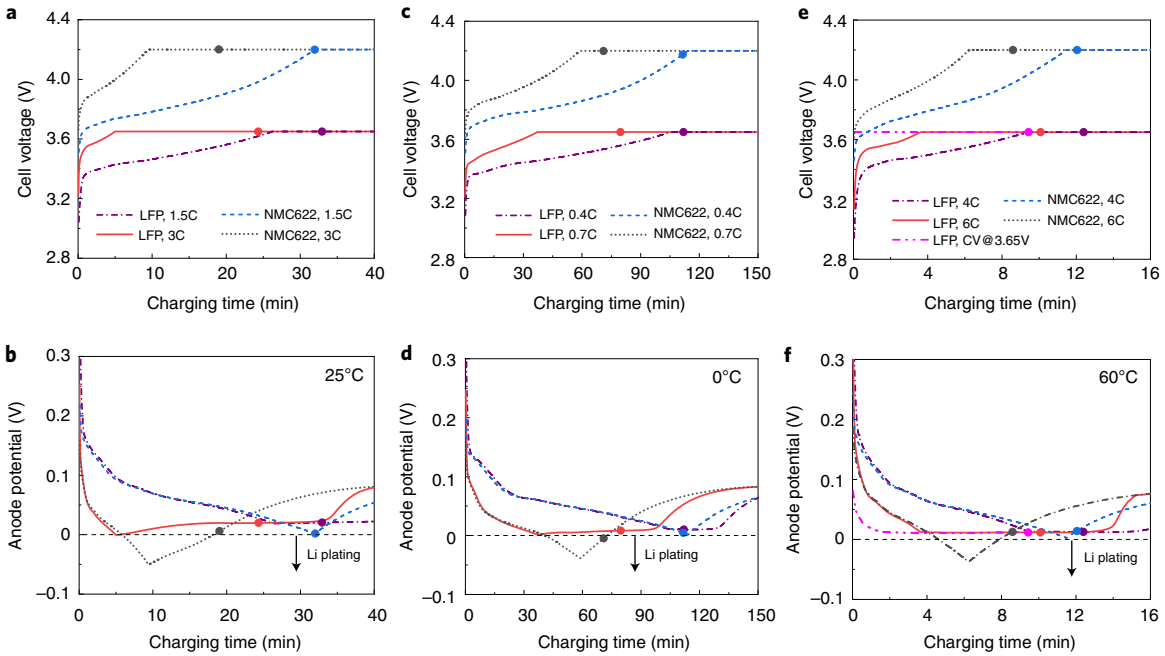

Fig. 4 | Fast-charging capability at different temperatures. a–f, The evolutions of cell voltage (**a**,**c**,**e**) and anode potential (**b**,**d**,**f**) (at the anode–separator interface) during charging of the blade-type graphite-LFP cell and the prismatic-type (VDA-BEV2 standard) graphite-NMC622 cell at different charge rates and temperatures: 25 °C (**a**,**b**), 0 °C (**c**,**d**), 60 °C (**e**,**f**). The cells are initially at 0% SOC, and the solid circles denote the time of reaching 80% SOC. The LFP and NMC622 cells follow the design information in Supplementary Table 2.

the power at 20 °C) owing to the enhanced electrochemical reactions and transport processes. Even at 10% SOC, the specific power of the TM-LFP battery still meets the target set forth by the EUCAR on peak specific power for 2030 mass-market EVs (Fig. 5b).

Third, the TM-LFP battery enables weather-independent fast charging in 10 min (Fig. 5c). As noted above, the PF-MCR of a lithium ion cell drops dramatically with the decrease of temperature due to the issue of lithium plating (Supplementary Fig. 10), leading to an increase of charging time (0 to 80% SOC) from 30 min at 20 °C to 80 min at 0 °C for the regular LFP blade cell. By elevating cell temperature to 60 °C, the same LFP cell can withstand the most aggressive protocol of CV charging at 3.65 V throughout the process and yields no lithium plating (Fig. 4f), cutting the charging time to 9.4 min. If using the more standard CCCV protocol at 6C rate, it still only takes 10.1 min (Fig. 4e). More importantly, such a fast charging can be performed at all ambient temperatures using the heated-charging approach presented in our recent works[35,36]. Even if the cell is initially at −30 °C, the total time of charging to 80% SOC would be only 10.9 min (1.5 min for heating from −30 °C to 60 °C plus 9.4 min for charging). The all-climate medium cruise range and readily extendable through 10 min fast charging, as offered by the TM-LFP battery, can enable EVs ultimately free of range anxiety. Also note that 6C charging of the 40 kWh TM-LFP batteries needs 240 kW chargers, which are readily available through Telsa V3 Supercharger Network or the 350 kW fast-charge stations recently installed by Electrify America. Most excitingly, the 40 kWh TM-LFP battery for a passenger EV free of range anxiety already exceeds cost parity with ICE vehicles.

Fourth, the elevated temperature also greatly reduces battery cooling need and thereby simplifies or even eliminates the battery thermal management system (BTMS). The heat balance of a battery cell can be mathematically expressed as:

$$I^2R = h(T_{\mathrm{cell}} - T_{\mathrm{amb}}) \quad (1)$$

where the left-hand-side represents heat generation rate, with I the current and R the cell internal resistance, whereas the right-hand-side represents the heat dissipation rate, with h the heat transfer coefficient and T_{cell} and T_{amb} the cell and ambient temperatures, respectively. As shown in Fig. 5b, the 10 s peak power (at 2.4 V constant voltage) of the LFP cell at 60 °C is about double of that at 25 °C, meaning that the internal cell resistance at 60 °C is about half of that at 25 °C. As such, the heat generation is reduced by half as cell temperature rises from 25 °C to 60 °C. On the other end, the driving force for heat dissipation ($T_{\mathrm{cell}} - T_{\mathrm{amb}}$) is enlarged to 35 °C ($T_{\mathrm{cell}}$ at 60 °C and T_{amb} at 25 °C). Assuming that a conventional BTMS can maintain cell temperature at 30 °C (that is, 5 °C temperature difference for cooling) in regular operation, the strategy of operating at 60 °C boosts the term $T_{\mathrm{cell}} - T_{\mathrm{amb}}$ by seven-fold. Together with the halved heat generation, the value of h for a TM-LFP battery is reduced to one-fourteenth of that for a regular battery pack. In this context, passive air cooling, instead of active liquid cooling, could suffice for a TM-LFP battery pack. Such a simplified BTMS can further improve pack-level energy density and reduce pack cost (for example, a current liquid cooling system accounts for ~5% of battery pack weight[39] and costs around US$250 for a 60 kWh pack[40]).

Million-mile EV Lifespan

In the past, it was believed that lithium-ion cells should avoid operating at high temperatures due to the concern of accelerated degradation. We recently revealed that cell aging driven by a high temperature depends on the time of the cell at the high temperature[35]. For a TM-LFP battery, it is exposed to 60 °C only during operation, which is a small fraction of the lifetime of an EV. According to the American Automobile Association[41], Americans spend about 51 min behind the wheel per day travelling for 31.5 miles (an average speed of 37 mph); thus, the time of an EV on the road, or of a TM-LFP battery at 60 °C, is only 3.5% (51 min out of 24 h) of a vehicle's lifespan. We should also note that LFP materials are particularly suitable for high-temperature operation, given their superior thermal stability. The primary aging mechanism in a LFP cell is the growth of solid–electrolyte interphase (SEI) on graphite

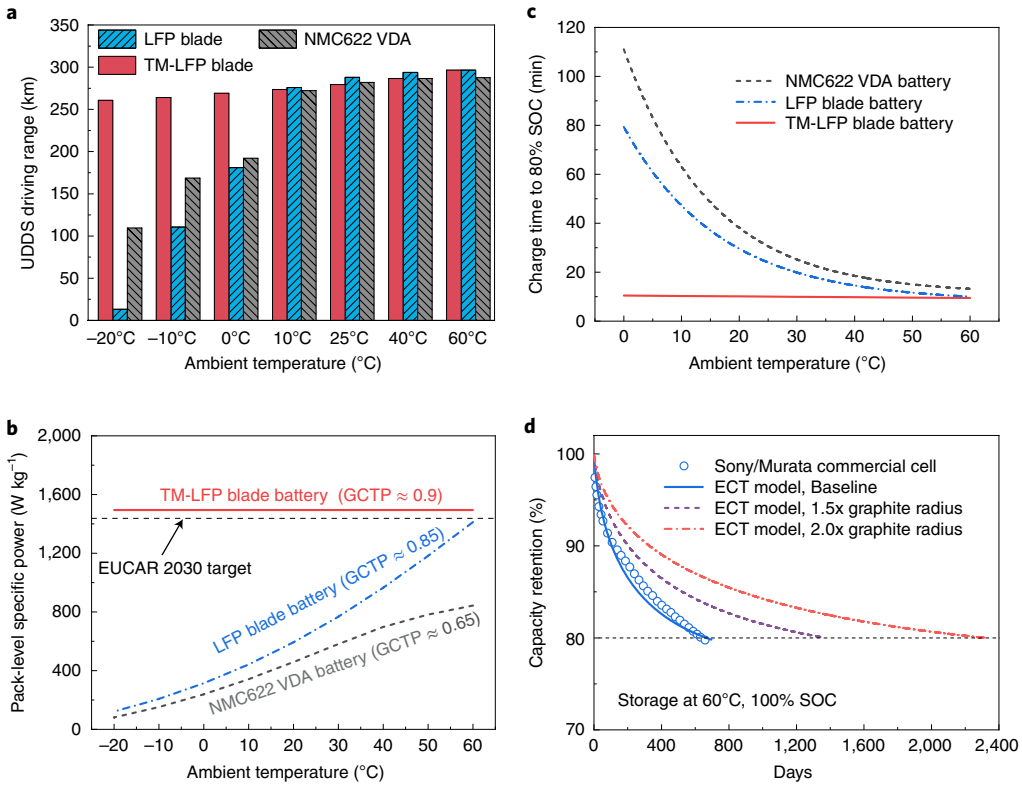

Fig. 5 | All-climate cruise range, remarkable power and 10 min fast charging with a TM-LFP blade battery. a–c, Comparisons of the TM-LFP blade battery with the regular LFP blade battery and the conventional NMC622 prismatic battery (VDA-BEV2 standard) in terms of: cruise range under the UDDS at different ambient temperatures for an EV with a 40 kWh battery composed of either of the three types of cells (**a**); pack-level specific power at 10% SOC (**b**); and the minimum time to charge from 0 to 80% SOC without lithium plating (**c**). The TM-LFP blade battery is preheated from ambient temperature to 60 °C before an operation, which consumes 1.35% SOC per 10 °C temperature rise (used for calculating the initial SOC in Fig. 5a; for instance, the TM-LFP battery at 25 °C starts at 95.3% SOC). The heating speed is 1 °C per second, and the heating time is included in the charging time of the TM-LFP battery shown in Fig. 5c. **d**, The calendar life of a graphite-LFP battery with different graphite particle sizes at 60 °C and 100% SOC. The solid symbols represent the experimental data from the literature on a commercial cell, and the lines are results predicted by a calibrated ECT aging model (see Supplementary Fig. 13).

surfaces, which is mainly a function of temperature, SOC and time. Supplementary Fig. 13 presents the calendar-life data of a widely utilized commercial graphite-LFP cell from Sony[42]. Even at 100% SOC, the fastest SEI growth scenario, the cell at 60 °C still has a lifetime (at 20% capacity loss) of 660 days. For a TM-LFP battery, a total of 660 day operating time at 60 °C represents a lifespan of 51 years and 586,080 miles (based on 51 min driving time a day at an average speed of 37 mph).

As the SEI growth rate is proportional to the BET area of graphite (equation (9))[43], the lifetime of a TM-LFP battery can be further enhanced by using graphite with low BET areas (for example, larger particles). In the past, low-BET-area graphite was not typically used in EV batteries, as a reduced surface area increases charge transfer resistance and larger particles lead to higher diffusion resistance. Elevating cell temperature from 20 °C to 60 °C can boost graphite reaction kinetics by 12-fold and graphite solid-state diffusivity 5.6-fold (Supplementary Fig. 11), effectively mitigating the adverse effects due to a reduced BET area. As shown in Supplementary Fig. 14, the increase of graphite particle size has minimal impacts on the cruise range of a TM-LFP battery-powered EV under either the UDDS or US06 protocol (Supplementary Fig. 14a), and a cell with two times the graphite radius at 60 °C even has better peak power than the baseline cell at 20 °C (Supplementary Fig. 14b). Regarding fast charging, a cell with 1.5 times the graphite radius can still be safely (without lithium plating) charged with the 6C current and 3.65 V cutoff voltage of the CCCV protocol at 60 °C and takes 10.3 min to charge from 0 to 80% SOC (Supplementary Fig. 14c,d), and the cell with two times the graphite radius can be charged to 80% SOC in 11.8 min with 6 C rate and a lower cutoff voltage of 3.6 V (to prevent lithium plating). These results demonstrate that the elevated temperature of 60 °C makes the performance of a TM-LFP cell insensitive to graphite particle radius. On the other hand, the particle size of graphite has a considerable impact on SEI growth at 60 °C. As shown in Fig. 5d, the calendar life at 20% capacity loss of the above-mentioned graphite-LFP cell at 60 °C and 100% SOC can be prolonged to 1,368 days with a 1.5 times the graphite radius, which, based on an average speed of 37 mph, corresponds to greater than 1.2 million driving miles for a TM-LFP battery-powered EV. If the graphite radius is doubled, the lifetime at 60 °C and 100% SOC soars further to 2,315 days, corresponding to greater than two million miles.

It is understood that battery cycling may cause additional degradation due to lithium insertion and extraction (for example, active material particle cracking). Dahn et al[44,45]. showed that the cycling-induced loss is however lessened at high temperatures and that the capacity loss of cells under cycling and storage almost overlap in the time domain at >40 °C. Schimpe et al[46] compared the capacity loss of the Sony/Murata LFP cells during cycling and storage and found that the pure cycling-induced loss follows a square-root dependency on an equivalent full cycle (EFC). By extrapolating their data (at 55 °C) and assuming 300 miles per EFC, we estimate a ~10% additional capacity loss after two million miles (~6,700 EFCs). Even when adding this cycling-induced loss, the TM-LFP battery with double the graphite radius is still projected to

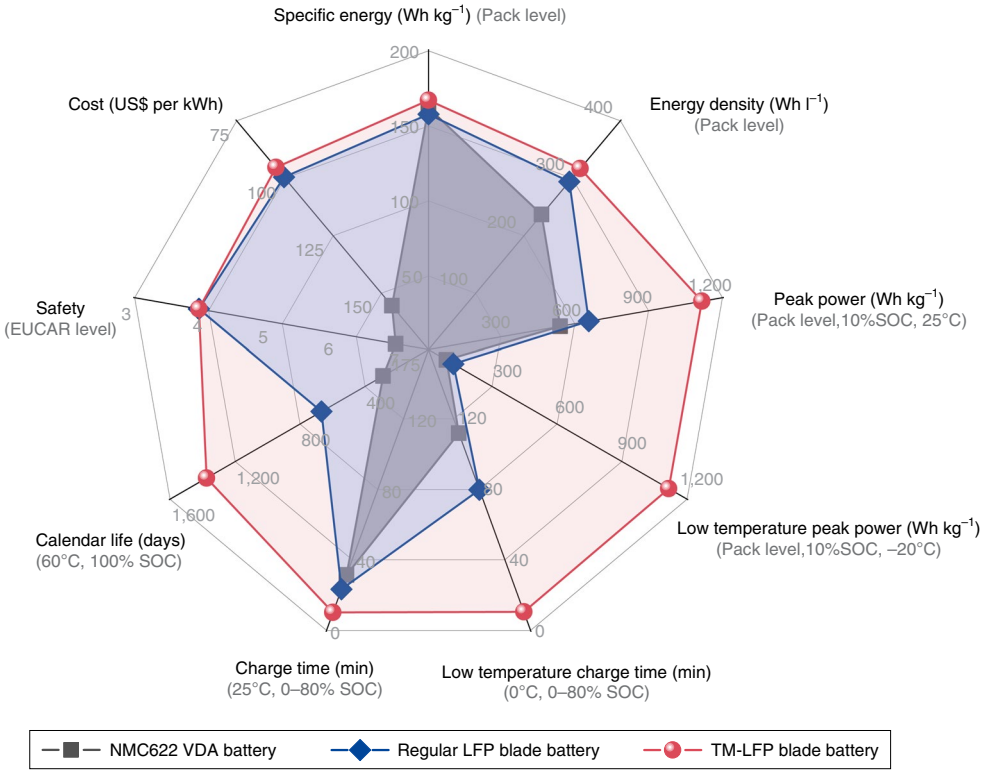

Fig. 6 | TM LFP blade battery fulfils all main criteria required for mass-market EVs. Comparisons of the TM-LFP blade battery (red), regular LFP blade battery (blue) and NMC622 prismatic battery (grey, VDA-BEV2 standard) under various performance criteria. The cells have an areal capacity of 3 mAh cm^{-2} (Supplementary Table 2). The specific energy and power are at the pack level, assuming a GCTP of 0.65 for the NMC622 battery, 0.85 for the regular LFP blade battery and 0.9 for the TM-LFP blade battery (with a simplified thermal management system). The temperatures in this figure refer to ambient temperatures. The TM-LFP battery refers to the cell with 1.5 times the graphite radius. The data points are from Fig. 2b for specific energy, Fig. 2d for energy density, Supplementary Figs. 5f and 14b for peak power, Fig. 4 and Supplementary Fig. 14d for charge time, and Fig. 5d for calendar life. The safety data are based on the EUCAR safety levels defined in ref. [32]. The battery cost are based on ref. [3] for an NMC battery and ref. [24] for a LFP battery, and the TM-LFP battery can further reduce cost by simplifying battery thermal management system (~US$250 for a 60 kWh battery pack[40]).

retain ~70% capacity after two million miles, which is greater than 16 times the warranty on many commercial EV batteries (for example, Tesla Model 3, 70% capacity for eight years or 120,000 miles). The TM-LFP battery therefore offers an opportunity to use graphite of low BET areas, enabling high performance and long lifetime simultaneously.

Conclusions

Figure 6 summarizes the performance metrics of the above three batteries: the NMC622 VDA battery, the regular LFP blade battery and the TM-LFP blade battery. With the improved CTP ratios, the LFP blade battery delivers comparable specific energy and better energy density at the pack level to the conventional NMC battery, offering a medium cruise range for passenger EVs at warm temperatures; LFP cells can also be charged faster than NMC cells due to a lower cutoff voltage, which helps prevent lithium plating. The primary challenge to LFP blade batteries for use in passenger EVs is the sharp reduction in cruise range at low temperatures, along with a drop in peak power and PF-MCR. Designed for operating at 60 °C in any ambient conditions, the TM-LFP battery not only tackles the issues at low temperatures but further boosts battery power and fast charging ability, leading to adequate cruise range coupled with 10 min fast recharge in all weather conditions. The elevated temperature also simplifies BTMS due to a 14-fold reduction in battery cooling need, which further enhances CTP efficiency and reduces cost. Moreover, the elevated operating temperature with a limited exposure time presents a way to achieving high performance and long lifetime simultaneously and makes it viable for using graphite of low BET areas, which can prospectively prolong the lifetime of an EV to over two million miles.

The world is currently at the inflection point of massive EV penetration. The TM-LFP blade battery presented in this work offers adequate cruise range per charge that is readily extendable through a 10 min recharge, and does so in all climates. We believe that such a TM-LFP battery is a viable alternative to energy-dense NMC/NCA batteries or carrying big batteries (for example, 100 kWh) on board to free EVs from range anxiety. Furthermore, the LFP battery enjoys unsurpassed advantages in safety, cost and containing no cobalt or nickel. Figure 6 shows that the TM-LFP battery can fulfil all major criteria required for EVs, presenting enormous potential for large-scale adoption in mass-market passenger EVs.

Methods

ECT model. The physics-based ECT model solves the following governing equations:

$$\text{Charge conservation in solid electrodes:} \quad \nabla \cdot \left(\sigma_s \nabla \phi_s\right) = j_{tot} \tag{2}$$

where ϕ_s is the solid-phase potential, σ_s is the electronic conductivity of the solid and j_{tot} is the total volumetric current density.

$$\text{Charge conservation in electrolyte:} \quad \nabla \cdot \left(\kappa_e \nabla \phi_e\right) + \nabla \cdot \left(\kappa_D \nabla \ln c_e\right) = -j_{tot} \tag{3}$$

where ϕ_e is the electrolyte-phase potential, κ_e and κ_D are the ionic conductivity and diffusional ionic conductivity of the electrolyte, respectively, and c_e is the concentration of the electrolyte.

$$\text{Mass conservation in electrolyte:} \quad \frac{\partial(\varepsilon c_e)}{\partial t} = \nabla \cdot (D_e \nabla c_e) + \frac{1 - t_+}{F} j_{tot} \tag{4}$$

where ε is electrode porosity, t is time, D_e is the diffusivity of the electrolyte, t_+ the transference number and F is the Faraday constant.

$$\text{Mass conservation in active materials:} \quad \frac{\partial c_s}{\partial t} = \frac{1}{r^2}\frac{\partial}{\partial r}\left(D_s r^2 \frac{\partial c_s}{\partial r}\right) \tag{5}$$

where c_s and D_s are the lithium concentration and diffusivity in solid active materials, respectively, and r is the particle radius.

$$\text{Energy conservation:} \quad mC_p \frac{dT}{dt} = Q + hA(T - T_{amb}) \tag{6}$$

where T is cell temperature, m, C_p and A are cell mass, thermal capacity and surface area, respectively, Q is heat generation rate, h is heat transfer coefficient, and T_{amb} is ambient temperature.

The total volumetric current density, j_{tot}, is the sum of the current density of the main and side reactions. The main reaction here refers to lithium intercalation/deintercalation, whose current density is calculated by the Butler–Volmer equation:

$$j_m = a i_{0,m}\left[\exp\left(\frac{\alpha_a F}{RT}\eta_m\right) - \exp\left(-\frac{\alpha_c F}{RT}\eta_m\right)\right] \tag{7}$$

where $i_{0,m}$ and η_m are the exchange current density and overpotential of the main reactions, respectively, α_a and α_c are the anodic and cathodic charge transfer coefficients, and a is the specific surface area (BET area), which depends on the volume fraction (ε_{AM}) and r of the active materials (AM):

$$a = \frac{3\varepsilon_{AM}}{r} \tag{8}$$

Solid–electrolyte interphase growth in the anode is considered as a side reaction in this model to account for cell aging, whose current density is calculated via the Tafel equation:

$$j_{SEI} = -aFk_{0,SEI}c_{EC}^{s}\exp\left(-\frac{\alpha_{c,SEI}F}{RT}\eta_{SEI}\right) \tag{9}$$

where $k_{0,SEI}$ is a kinetic rate constant and c_{EC}^{s} is the concentration of ethylene carbonate (EC) on the surface of graphite, which is calculated based on the mass conservation of EC:

$$-D_{EC}\frac{c_{EC}^{s} - c_{EC}^{bulk}}{\delta_{SEI}} = -\frac{j_{SEI}}{F} \tag{10}$$

where D_{EC} and c_{EC}^{bulk} are the diffusivity and bulk concentration of EC, respectively, and δ_{SEI} is the SEI layer thickness.

Model validation

The above model is used to predict the performance of two types of cells: a graphite-LFP cell and a graphite-NMC622 cell. We performed a set of validations to calibrate the model parameters to reasonably predict the characteristics of LFP and NMC622 cells. The model for the graphite-NMC622 cell was validated against the experimental data of a 10 Ah pouch cell presented in refs. [47,48], and the model for the graphite-LFP cell was validated against the data of a commercial 20 Ah cell given in refs. [49,50]. The model validation includes comparing with the experimental data of (1) charge and discharge with various C-rates at 25 °C and (2) charge and discharge with 1C rate at various ambient temperatures. As can be seen from Supplementary Figs. 1–4, both the cell voltage and temperature can be predicted reasonably well under all these conditions, demonstrating that the models can well capture the electrochemical and thermal behaviours of LFP and NMC622 cells. The calibrated models are then used to predict the performance of the blade-type graphite-LFP cell and the VDA-type graphite-NMC622 cell, following the cell design information in Supplementary Table 2.

The aging model is validated against the calendar aging data of a commercial graphite-LFP cell from Sony/Murata presented in ref. [42]. We can see from Supplementary Fig. 13 that the model well predicts the calendar life of the cell at various temperatures and SOCs. The calibrated model was then applied to predict the calendar life of cells with low BET-area graphite (Fig. 5d), changing only the radius of graphite particles.

Vehicle dynamics model

The vehicle dynamics model in ref. [51] is adopted to convert the US EPA-defined velocity profiles for the UDDS and US06 driving cycles to battery power profiles (Supplementary Fig. 7). Here we used the specifications of Nissan Leaf (with 40 kWh battery) to calculate the power at the wheels:

$$P_{wheels}(t) = \left(m_V \frac{dv(t)}{dt} + m_V g\cos(\theta)\frac{C_r}{1{,}000}(c_1 v(t) + c_2) + \frac{1}{2}\rho_{air}A_f C_D v^2(t) + m_V g\sin(\theta)\right)v(t) \tag{11}$$

where m_v is the vehicle mass (1,995 kg), $v(t)$ is the velocity (in metres per second), g is the gravity of Earth (9.8 m s^{-2}), θ is climbing angle (assumed to be 0), $C_r = 1.75$, $c_1 = 0.0328$ and $c_2 = 4.575$ are rolling resistance parameters, ρ_{air} is the air density (1.225 kg m^{-3}), A_f is the front area of the vehicle (2.7356 m^2) and C_D is the aerodynamic drag coefficient (0.28).

The power of the battery pack in traction and regenerative braking modes is then calculated as:

$$\text{Traction mode:} \quad P_{batt} = P_{wheels}/(\eta_T \eta_{md}) \tag{12a}$$

$$\text{Regenerative braking mode:} \quad P_{batt} = P_{wheels}\eta_{rb} \tag{12b}$$

where η_T is the transmission efficiency (92%), η_{md} is the efficiency of the electric motor (91%) and η_{rb} is the efficiency of regenerative braking (82%). The calculated battery pack power is divided by the number of cells in the pack to calculate the power of single cells, which is then implemented in the above ECT models. In this work we study a 40 kWh battery pack, which consists of either 62 of the 202 Ah LFP blade cells or 69 of the 158 Ah NMC622 VDA cells in Supplementary Table 2. The driving cycle power profiles are repeated until the single-cell voltage reaches the cutoff value (2.4 V for the LFP cell and 2.7 V for the NMC622 cell). The driving range shown in Figs. 3 and 5 are calculated by integrating the velocity profiles over time.

Data availability

All relevant data are included in the paper and its Supplementary Information. Source data are provided with this paper.

Code availability

The case files for the cell performance and degradation simulations on Autolion-1D v7.0 are publicly available at https://github.com/ECECPSU/TMLFP

Received: 3 August 2020; Accepted: 1 December 2020;
Published online: 18 January 2021

References

1. *Fast Facts: US Transportation Sector Greenhouse Gas Emissions (1990–2018)* (US EPA, 2019); https://nepis.epa.gov/Exe/ZyPDF.cgi?Dockey=P100ZK4P.pdf
2. Needell, Z. A., McNerney, J., Chang, M. T. & Trancik, J. E. Potential for widespread electrification of personal vehicle travel in the United States. *Nat. Energy* **1**, 16112 (2016).
3. *Electric Vehicle Outlook 2020* (BloombergNEF, 2020); https://about.bnef.com/electric-vehicle-outlook/
4. Lienert, P. & Chan, C. Global automakers investing at least $300 billion on batteries and EVs. *Reuters* (2019); https://graphics.reuters.com/AUTOS-INVESTMENT-ELECTRIC/010081ZB3HD/index.html
5. Whittingham, M. S. Lithium batteries and cathode materials. *Chem. Rev.* **104**, 4271–4302 (2004).
6. Nitta, N., Wu, F., Lee, J. T. & Yushin, G. Li-ion battery materials: present and future. *Mate. Today* **18**, 252–264 (2015).

7. Schmuch, R., Wagner, R., Hörpel, G., Placke, T. & Winter, M. Performance and cost of materials for lithium-based rechargeable automotive batteries. *Nat. Energy* **3**, 267–278 (2018).
8. Li, M., Lu, J., Chen, Z. & Amine, K. 30 Years of lithium-ion batteries. *Adv. Mater.* **30**, 1800561 (2018).
9. Ding, Y., Cano, Z. P., Yu, A., Lu, J. & Chen, Z. Automotive Li-ion batteries: current status and future perspectives. *Electrochem. Energy Rev.* **2**, 1–28 (2019).
10. Andre, D. et al. Future generations of cathode materials: an automotive industry perspective. *J. Mater. Chem. A* **3**, 6709–6732 (2015).
11. LFP market share drops in 2019 but expect a comeback with cell-to-pack. *Adamas Intelligence* (4 March 2020); https://www.adamasintel.com/lfp-market-2019-cell-to-pack-comeback/
12. Sun, Y.-K. et al. High-energy cathode material for long-life and safe lithium batteries. *Nat. Mater.* **8**, 320–324 (2009).
13. Olivetti, E. A., Ceder, G., Gaustad, G. G. & Fu, X. Lithium-ion battery supply chain considerations: analysis of potential bottlenecks in critical metals. *Joule* **1**, 229–243 (2017).
14. Manthiram, A., Knight, J. C., Myung, S.-T., Oh, S.-M. & Sun, Y.-K. Nickel-rich and lithium-rich layered oxide cathodes: progress and perspectives. *Adv. Energy Mater.* **6**, 1501010 (2016).
15. Manthiram, A., Song, B. & Li, W. A perspective on nickel-rich layered oxide cathodes for lithium-ion batteries. *Energy Storage Mater.* **6**, 125–139 (2017).
16. Xiong, R., Ma, S., Li, H., Sun, F. & Li, J. Toward a safer battery management system: a critical review on diagnosis and prognosis of battery short circuit. *iScience* **23**, 101010 (2020).
17. Feng, X., Ren, D., He, X. & Ouyang, M. Mitigating thermal runaway of lithium-ion batteries. *Joule* **4**, 743–770 (2020).
18. Noh, H.-J., Youn, S., Yoon, C. S. & Sun, Y.-K. Comparison of the structural and electrochemical properties of layered $Li[Ni_xCo_yMn_z]O_2$ ($x = 1/3$, 0.5, 0.6, 0.7, 0.8 and 0.85) cathode material for lithium-ion batteries. *J. Power Sources* **233**, 121–130 (2013).
19. Yamada, A., Chung, S. C. & Hinokuma, K. Optimized $LiFePO_4$ for lithium battery cathodes. *J. Electrochem. Soc.* **148**, A224 (2001).
20. Zaghib, K. et al. Enhanced thermal safety and high power performance of carbon-coated $LiFePO_4$ olivine cathode for Li-ion batteries. *J. Power Sources* **219**, 36–44 (2012).
21. Lamb, J., Torres-Castro, L., Stanley, J., Grosso, C. & Gray, L. S. *Evaluation of Multi-cell Failure Propagation* SAND-2020-2802 (Sandia National Laboratories, 2020); https://doi.org/10.2172/1605985
22. Wang, Z., Zhu, K., Hu, J. & Wang, J. Study on the fire risk associated with a failure of large-scale commercial $LiFePO_4$/graphite and $LiNi_xCo_yMn_{1-x-y}O_2$/graphite batteries. *Energy Sci. Eng.* **7**, 411–419 (2019).
23. *New Energy Vehicles Safety Monitoring Results Report* (National Big Data Alliance of New Energy Vehicles, 2019).
24. Morris, J. Tesla's shift to cobalt-free batteries is its most important move yet. *Forbes* (11 July 2020); https://www.forbes.com/sites/jamesmorris/2020/07/11/teslas-shift-to-cobalt-free-batteries-is-its-most-important-move-yet/
25. Mullaney, T. Tesla and the science behind the next-generation, lower-cost, 'million-mile' electric-car battery. *CNBC TECH TRENDS* (30 June 2020); https://www.cnbc.com/2020/06/30/tesla-and-the-science-of-low-cost-next-gen-ev-million-mile-battery.html
26. Takahashi, M., Ohtsuka, H., Akuto, K. & Sakurai, Y. Confirmation of long-term cyclability and high thermal stability of $LiFePO_4$ in prismatic lithium-ion cells. *J. Electrochem. Soc.* **152**, A899 (2005).
27. Wang, C., He, L., Sun, H., Lu, P. & Zhu, Y. Battery pack, vehicle and energy storage device. China Patent CN110165118B (2019).
28. He, K., Jiang, W., Wang, X. & Wen, A. Single battery, power battery pack and vehicle. China Patent CN110364675A (2019).
29. Jiang, L., Yang, K., Zhu, Y. & Zhu, J. Electric connector and battery comprising the same. United States Patent US20170346065A1 (2017).
30. Kwon, M., Choi, J., Kwon, K., Do, E. & Lee, Y. Complex electrode assembly including plurality of electrode assemblies and electrochemical device comprising the complex electrode assembly. United States Patent US20200020922A1 (2020).
31. Gallagher, K. G. et al. Optimizing areal capacities through understanding the limitations of lithium-ion electrodes. *J. Electrochem. Soc.* **163**, A138–A149 (2015).
32. *Battery Requirements for Future Automotive Applications* (EUCAR, 2019); https://eucar.be/wp-content/uploads/2019/08/20190710-EG-BEV-FCEV-Battery-requirements-FINAL.pdf
33. Dynamometer Drive Schedules. *United States Environmental Protection Agency* https://www.epa.gov/vehicle-and-fuel-emissions-testing/dynamometer-drive-schedules
34. Wang, C. Y. et al. Lithium-ion battery structure that self-heats at low temperatures. *Nature* **529**, 515–518 (2016).
35. Yang, X. G. et al. Asymmetric temperature modulation for extreme fast charging of lithium-ion batteries. *Joule* **3**, 3002–3019 (2019).
36. Yang, X. G., Zhang, G., Ge, S. & Wang, C. Y. Fast charging of lithium-ion batteries at all temperatures. *Proc. Natl Acad. Sci. USA* **115**, 7266–7271 (2018).
37. Yang, X. et al. All-climate battery technology for electric vehicles: inching closer to the mainstream adoption of automated driving. *IEEE Electrific. Mag.* **7**, 12–21 (2019).
38. Zhang, G. et al. Rapid self-heating and internal temperature sensing of lithium-ion batteries at low temperatures. *Electrochim. Acta* **218**, 149–155 (2016).
39. Nelson, P. A., Ahmed, S., Gallagher, K. G. & Dees, D. W. *Modeling the Performance and Cost of Lithium-Ion Batteries for Electric-Drive Vehicles* 3rd edn ANL/CSE-19/2 (Argonne National Laboratory, 2020).
40. Lutsey, N. & Nicholas, M. *Update on Electric Vehicle Costs in the United States Through 2030* 1–12 (International Council on Clean Transportation, 2019).
41. *Americans Spend an Average of 17,600 Minutes Driving Each Year* (American Automobile Association, 2016); https://newsroom.aaa.com/2016/09/americans-spend-average-17600-minutes-driving-year/
42. Naumann, M., Schimpe, M., Keil, P., Hesse, H. C. & Jossen, A. Analysis and modeling of calendar aging of a commercial $LiFePO_4$/graphite cell. *J. Energy Storage* **17**, 153–169 (2018).
43. Smith, A. J., Burns, J. C., Zhao, X., Xiong, D. & Dahn, J. R. A high precision coulometry study of the SEI growth in Li/graphite cells. *J. Electrochem. Soc.* **158**, A447 (2011).
44. Harlow, J. E. et al. A wide range of testing results on an excellent lithium-ion cell chemistry to be used as benchmarks for new battery technologies. *J. Electrochem. Soc.* **166**, A3031–A3044 (2019).
45. Cheng, J. H., Harlow, J. E., Johnson, M. B., Gauthier, R. & Dahn, J. R. Effect of duty cycle on the lifetime of single crystal $LiNi_{0.5}Mn_{0.3}Co_{0.2}O_2$/graphite lithium-ion cells. *J. Electrochem. Soc.* **167**, 130529 (2020).
46. Schimpe, M. et al. Comprehensive modeling of temperature-dependent degradation mechanisms in lithium iron phosphate batteries. *J. Electrochem. Soc.* **165**, A181–A193 (2018).
47. Wang, C. Y. et al. A fast rechargeable lithium-ion battery at subfreezing temperatures. *J. Electrochem. Soc.* **163**, A1944–A1950 (2016).
48. Yang, X. G., Leng, Y., Zhang, G., Ge, S. & Wang, C. Y. Modeling of lithium plating induced aging of lithium-ion batteries: transition from linear to nonlinear aging. *J. Power Sources* **360**, 28–40 (2017).
49. Mastali, M., Farkhondeh, M., Farhad, S., Fraser, R. A. & Fowler, M. Electrochemical modeling of commercial $LiFePO_4$ and graphite electrodes: kinetic and transport properties and their temperature dependence. *J. Electrochem. Soc.* **163**, A2803–A2816 (2016).
50. Mastali, M. et al. Electrochemical-thermal modeling and experimental validation of commercial graphite/$LiFePO_4$ pouch lithium-ion batteries. *Int. J. Therm. Sci.* **129**, 218–230 (2018).
51. Fiori, C., Ahn, K. & Rakha, H. A. Power-based electric vehicle energy consumption model: model development and validation. *Appl. Energy* **168**, 257–268 (2016).

Acknowledgements

Financial support from the US Department of Energy's Office of Energy Efficiency and Renewable Energy (EERE) under award no. DE-EE0008355 and the William E. Diefenderfer Endowment is gratefully acknowledged. We are also grateful to Gamma Technologies for providing licences to GT-Autolion software, with which we performed the ECT modelling.

Author contributions

X.G.Y and C.Y.W. conceived the idea and wrote the manuscript. X.G.Y. designed and performed the modelling studies. All authors contributed to analyses of the results.

Competing interests

The authors declare no competing interests.

Additional information

Supplementary information is available for this paper at https://doi.org/10.1038/s41560-020-00757-7.

Correspondence and requests for materials should be addressed to C.-Y.W.

Peer review information *Nature Energy* thanks Partha Mukherjee, Kandler Smith and Karim Zaghib for their contribution to the peer review of this work.

Reprints and permissions information is available at www.nature.com/reprints.

Publisher's note Springer Nature remains neutral with regard to jurisdictional claims in published maps and institutional affiliations.